Tuning Polymer Light-Emitting Device Emission Colors in Ternary Blends Composed of Conjugated and Nonconjugated Polymers

Nisha Ananthakrishnan,[†] G. Padmanaban,[‡] S. Ramakrishnan,[‡] and John R. Reynolds*,[†]

The George and Josephine Butler Polymer Research Laboratory, Department of Chemistry, Center for Macromolecular Science and Engineering, University of Florida, Gainesville, Florida 32611-7200, and Department of Inorganic and Physical Chemistry, Indian Institute of Science, Bangalore, 560 012, India

Received April 13, 2005; Revised Manuscript Received June 29, 2005

ABSTRACT: We report here the utilization of a ternary polymer blend system consisting of two conjugated polymers, the orange emitting poly(2-methoxy-5-(2′-ethyl-hexyloxy)-*p*-phenylenevinylene) (MEH-PPV) and blue emitting poly(9,9-dioctylfluorene) (PFO), with the inert matrix polymer poly(methyl methacrylate) (PMMA) to show voltage-controlled color tuning in micro- and nano-phase-separated domains. Morphological characterization using atomic force microscopy showed 100−600 nm diameter sized conjugated polymer domains depressed into the surface when processed from toluene. Fluorescence microscopy and transmission electron microscopy were utilized to show that the conjugated polymers, present as the minority phase relative to PMMA, tend to remain together in domains phase separated from the matrix. Photophysical and electroluminescence studies showed efficient Förster energy transfer from PFO to MEH-PPV when equal concentrations of conjugated polymers were utilized with emission occurring at 570 nm, leading to a bright yellow light-emitting device. Ternary blends containing an excess of PFO relative to MEH-PPV showed voltage tunable (8−12 V) yellow to green electroluminescence. The ternary blend devices showed higher efficiencies than the binary blend devices consisting of PFO/PMMA. These results demonstrate that the phase-separated morphology having an excess of the high band gap polymer is essential for obtaining voltage-controlled variable color emission in polymer light-emitting devices.

Introduction

Conjugated polymers have been utilized in the field of polymer light-emitting diodes (PLEDs) since the discovery of this property in the early 1990s.[1,2] The field has progressed rapidly, and PLEDs can now be prepared across the entire visible spectrum and have reached commercial availability.[3,4] The attractive feature of these polymers is their ability to form thin films from solution by spin-coating. This avoids the need for high-vacuum deposition, allows devices to be constructed on flexible substrates, and extends their application to display systems. One area of emphasis has been the possibility for patterning and control of colors in PLEDs. Some approaches used for color tuning include variation of polarity and voltage,[5] multilayer device architectures,[6] changing substituents and substitution patterns on the conjugated polymer chain,[7] conjugation length control,[8] and copolymerization with dyes.[9]

The most simple, cost-effective, and common approach has been to utilize polymer blends[10] for color conversion and white light emission.[11,12] Intimate interaction between two conjugated polymers in a blend can lead to energy transfer[13,14] from host to guest as in the case of blue emitting poly(9,9-dioctylfluorene) (PFO) with green emitting poly(9,9-dioctylfluorene-*alt*-benzothiadiazole) (F8BT) which gives a green emission.[15] In other examples, polymer blends can emit with an entirely different observed color than the individual components as in the case of poly(3-hexylthiophene) (P3HT) and poly(*N*-vinylcarbazole) (PVK) which emits with a light violet color (a mixture of blue and red).[16,17]

One approach to variable color emission which has been harnessed to a great extent is voltage tunable multicolor PLEDs.[18−22] In early work, this objective was achieved by synthesizing polythiophenes with different substituents on the main chain to yield materials having emissions ranging from blue to red. Blends of these polythiophene derivatives[21,22] were then used to obtain voltage-controlled variable color light sources. Blends of polymers with different electronic characteristics, such as the p-type polymer poly(*p*-phenylenevinylene) with the n-type polymer poly(2,6-(4-phenyl)quinoline) (PPQ),[19,20] have also been useful in creating multicolor emission ranging from red to green with an increase of device voltage.

In a regular PLED, electrons are injected into the LUMO and holes into the HOMO of the conjugated polymer. The resulting charges migrate under the influence of the electric field and recombine to form an exciton which emits light. It is relatively straightforward to extend this to developing an understanding of voltage tunable color emission in PLED blends based on the fundamental processes in Scheme 1 for a combination of high band gap and low band gap polymers.

Two types of conjugated polymer blends composed of materials with different band gaps are considered: (1) miscible blends (no phase separation at a given temperature and composition) of the two polymers alone and (2) phase-separated blends created by the two polymers inherent incompatibility[20] or due to the presence of an inert polymer matrix which serves to separate the light-emitting domains.

In the first case (1), two possibilities can occur. First, injection of holes and electrons can occur into the HOMO and LUMO, respectively, of the higher band gap polymer, followed by Förster energy transfer to the

[†] University of Florida.
[‡] Indian Institute of Science.
* Corresponding author. E-mail reynolds@chem.ufl.edu.

10.1021/ma050787j CCC: $30.25
Published on Web 08/12/2005

Scheme 1

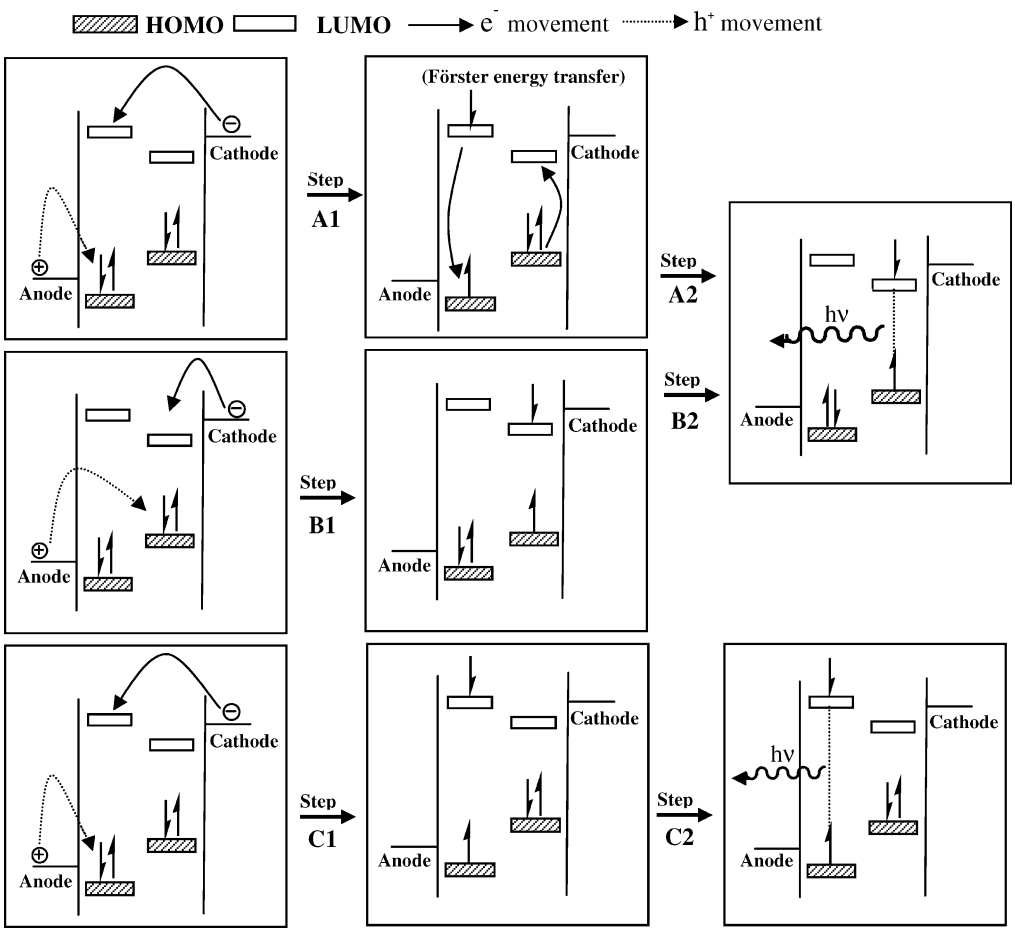

lower band gap polymer[23,24] and subsequent emission as shown by steps A1 and A2 in Scheme 1. Alternatively, direct injection of charges into the HOMO and LUMO of the low band gap polymer, as illustrated by steps B1 and B2, leads to the same emission.[25] It is also possible that the hole may be injected in the HOMO level of the low band gap polymer and the electron in the LUMO level of the high band gap polymer, or vice versa, depending upon their position with respect to the injecting electrodes. In both the cases, the charges may migrate into the high band gap polymer leading to steps A1 and A2 or to the low band gap polymer leading to steps B1 and B2. Förster energy transfer is favored when there is good spectral overlap between the donor's (high band gap polymer) emission and the acceptor's (low band gap polymer) absorption and when the HOMO and LUMO energy levels of the acceptor are nested within the band gap of the donor. As such, in a miscible polymer blend, it is only possible to obtain emission color change by blending varied amounts of the low and high band gap polymers.[24]

In the second case (2), energy transfer from the higher- to lower band gap polymer may be incomplete due to the presence of phase-separated domains of light-emitting polymer leading to emission from both polymers as shown when steps C1 and C2 occur simultaneously with B1 and B2 and recombination occurs on both polymers. It is also seen that the barriers to the injection of both electrons and holes increase for a high band gap polymer with a given set of electrodes having work functions which are well-matched with the low band gap polymer.[26] In such a case, the high band gap polymer emits only at higher voltages.[21] As such, it is possible to have voltage controlled color tuning in polymer blends if there is a higher composition of the high band gap polymer relative to the low gap polymer and/or phase separation between the emitting polymers.

Polymer/polymer blends, where the major component is an inert polymer such as polystyrene (PS)[27] or poly(methyl methacrylate) (PMMA), with a conjugated polymer forming the minor component have been utilized to form nano-LEDs[28,29] with emitting domains on the order of 300−500 nm. We have shown the compositional evolution of morphology[30] of blends consisting poly(2-methoxy-5-(2′-ethylhexyloxy)-*p*-phenylenevinylene) (MEH-PPV) with PMMA. At low concentrations of MEH-PPV, isolated light-emitting domains ranging in diameter from 300 to 900 nm were observed. To a limited extent such phase-separated structures can be utilized to provide especially small light sources which may prove useful in optical microscopic methods.[31]

Here, we report the utilization of a ternary polymer blend system consisting of two conjugated polymers, the orange emitting MEH-PPV[32] and blue emitting PFO, with the inert polymer PMMA to demonstrate voltage controlled color tuning in micro- and nanophase-separated domains. Previously, blends of PFO with MEH-PPV[33] without the matrix polymer were investigated, and the authors showed yellow color emission at 570 nm due to energy transfer with reduction in full width at half-maximum (fwhm) when 4 wt % of MEH-PPV was used. At this concentration, no phase separation was observed using atomic force microscopy (AFM) phase images and a smooth, homogeneous film was observed. In our work, we show detailed characterization of ternary polymer blend morphology with its effect

on light emission characteristics. The phase-separated morphology of the ternary blends showed 100−500 nm domains containing both conjugated polymers as investigated by AFM, fluorescence microscopy, and transmission electron microscopy (TEM). A combined photophysical and electroluminescence study of polymer films and LEDs showed that relative composition difference between the conjugated polymers determines the emission colors. It is shown that voltage-induced color tuning takes place even though the conjugated polymers are present together in a single microdomain and are phase-separated from the matrix polymer. An equal concentration of the two conjugated polymers in PMMA led to a bright yellow emitting LED, while an unequal composition of the conjugated polymers with excess PFO caused a color change from yellow to green with an increase in voltage.

Results and Discussion

The miscibility of polymers depends on the free energy of mixing which in turn depends on both enthalpic and entropic contributions. In the case of ternary polymer blend systems the enthalpic interactions between each of the polymer components determines the extent of phase separation in terms of morphology and domain size.[34] Spin-coating of the polymers from a common solvent also results in nonequilibrium morphologies as it is too rapid for equilibrium to be obtained.[35] For a system containing two conjugated polymers (CP_1 and CP_2) as minority phases dispersed in a majority component or matrix polymer (MP), six different lateral phase-separated morphologies can be considered. In the case where the two conjugated polymers do not mix, they can independently bloom from, or depress into, the surface providing four different possible structures. In a second case where the two conjugated polymers do intimately mix, both CP_1 and CP_2 will be present together in a single phase and will depress into or bloom from the surface with respect to the MP. The elevation or depression of each phase relative to the MP is due to the differences in solubility parameters between the components in a common solvent. During spin-coating the least soluble component tends to separate from the homogeneous spin solution and solidifies first, moving to the air:film interface minimizing the interaction of that polymer with the solvent and leading to elevation of that polymer on the surface.

Binary Polymer Blend Morphology. In the present case of MEH-PPV and PFO dispersed in PMMA the solubility parameters of the conjugated polymers are similar to toluene, and they tend to remain together in a single depressed conjugated polymer blend phase while the matrix polymer blooms to the surface as illustrated by the AFM results of Figure 1. The solubility of a given polymer in a solvent is largely determined by its chemical structure where structural similarity favors solubility and is favored if the solubility parameters (δ) of polymer and solvent are similar. The solubility parameters of PMMA, MEH-PPV, PFO, and toluene were calculated using group contribution methods with data tables of Hoftyzer and Van Krevelen[36] and depend on three main factors: (a) contribution from dispersion forces (δ_d), (b) contribution of polar forces (δ_p), and (c) contribution of hydrogen bonding (δ_h). The results predict that toluene ($\delta = 17.6 \pm 1 (J/cm^3)^{1/2}$) will be a better solvent for MEH-PPV ($\delta = 18.0 \pm 1$ $(J/cm^3)^{1/2}$) and PFO ($\delta = 17.2 \pm 1$ $(J/cm^3)^{1/2}$) than for PMMA ($\delta = 20.5 \pm 1$ $(J/cm^3)^{1/2}$), supporting the trend seen in our results. The main focus of the research reported here is to demonstrate the effect of polymer blend composition on the light-emitting characteristics of a phase-separated ternary polymer blend system. In PLEDs, interfaces play a crucial role as hole injection at the anode (often poly(3,4-ethylenedioxythiophene)/poly(styrenesulfonate) (PEDOT/PSS)-coated ITO) and electron injection at a low work function metal cathode are required in order to form the emitting excited state. As such, all of the investigations reported here are carried out on polymer blend films, which have been spin-coated onto a thin layer of PEDOT/PSS (ca. 45 nm) on cleaned glass. The light-emitting films develop their morphology on the PEDOT/PSS, and thus this morphology is equivalent to that obtained in the LEDs themselves. In order to determine control morphologies of binary blends, the results of Figure 1a,d show the tapping mode AFM images of ∼80−100 nm thick spin-cast films of 8 wt % MEH-PPV in PMMA and 8 wt % PFO in PMMA from a toluene solution.

The surface morphology shows 400−500 nm domains depressed down into the surface in each case. Previously, we reported that the morphology of 5−25 wt % MEH-PPV in PMMA spin-coated from 1,2-dichloroethane (DCE) lead to 300−900 nm sized light-emitting domains blooming from the surface.[30] In the current study, the surface characteristics are reversed with the aromatic solvent toluene, and this is attributed to the fact that PMMA tends to dissolve better in the polar solvent DCE ($\delta = 21.0 \pm 1$ $(J/cm^3)^{1/2}$). During the spin-coating process in DCE, PMMA tends to retain solvent longer than MEH-PPV, causing the conjugated polymer to bloom to the surface. When toluene is used, PMMA is deprived of the solvent faster than MEH-PPV, and it tends to protrude upward instead. This evolution of structures with change in solvent has also been studied in cases of nonconjugated polymer blends including PMMA/PS[37] and deuterated polystyrene−polybromostyrene blend systems.[38] The morphology obtained for low compositions of PFO in PMMA with toluene as solvent was similar to that of the MEH-PPV/PMMA system. This shows that the solubility characteristics of PFO are similar to that of MEH-PPV in accordance to the calculations discussed above. The morphology of the PFO/PMMA system was also studied by Chappel et al. using near-field scanning microscopy, and similar morphology results were obtained.[39]

Ternary Polymer Blend Morphology and Phase Compositions. Figure 1b,c shows the tapping mode topographic and phase images of the ternary blends of MEH-PPV and PFO in PMMA with equal composition of the conjugated polymers (4:4 wt %) and an excess of PFO (1:7 wt %). It is noted that they have a similar lateral topography as the binary blends. The photophysical, emission, and morphological properties of the 3:5 and 2:6 wt % MEH-PPV:PFO in PMMA were similar to the 4:4 wt % of MEH-PPV:PFO, while the 1:7 wt % blend showed different properties allowing us to focus on the latter two compositions. During spin-coating, the PMMA being least soluble solidifies first, and the solvent can then evaporate simultaneously, leaving the two components trapped in a domain.

This is confirmed by the results of Figure 2, where we show for the first time the utilization of fluorescence microscopy for a ternary blend system to delineate location of two conjugated polymers in a matrix polymer.

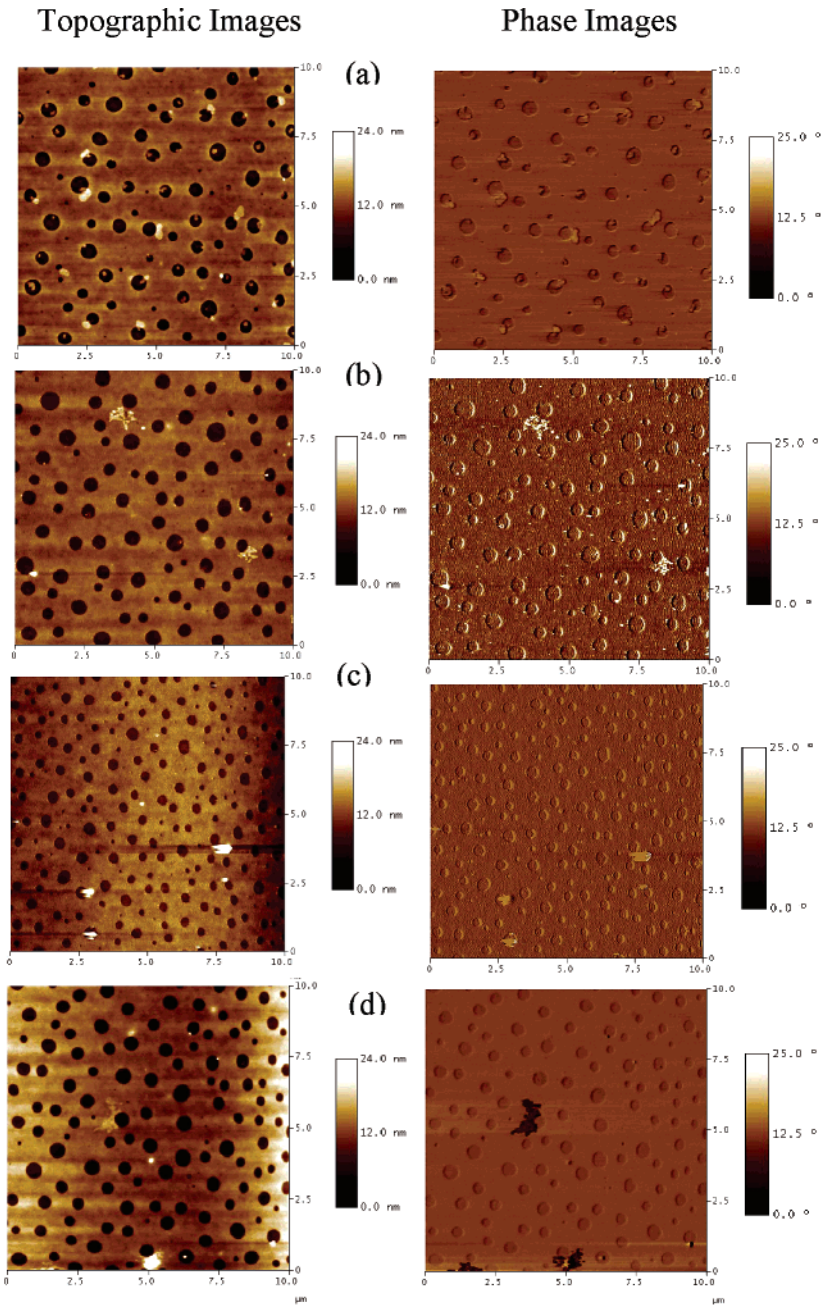

Figure 1. AFM topographic and phase images of (a) 8 wt % of MEH-PPV in PMMA, (b) 4:4 wt % of MEH-PPV:PFO in PMMA, (c) 1:7 wt % of MEH-PPV:PFO in PMMA, and (d) 8 wt % PFO in PMMA.

In this experiment, the 1:7 wt % film was first excited with ultraviolet light (360 nm band-pass ± 60 nm) and observed using a blue-violet transmitting (450 nm band-pass ± 40 nm) filter (Figure 2a), where domains of 500−600 nm in diameter fluoresce indicating the presence of PFO.

When the same section of the film was excited with blue light (425 nm band-pass ± 40 nm) and observed using a red transmitting (630 nm band-pass ± 60 nm) filter in Figure 2b, *the same domains fluoresce*, indicating the presence of MEH-PPV. These morphological studies prove that the conjugated polymers present as the minority phase relative to PMMA remain together upon phase separation. Essentially identical micrographs were obtained when a 4:4 wt % blend was examined under the same conditions. In a control experiment, the AFM topography of binary blends of MEH-PPV and PFO without the matrix polymer showed no phase separation with a 50−200 nm resolution at 10, 25, and 50 wt % of MEH-PPV in PFO. Domains of 20−80 nm in size were observed at 75 and 90 wt % of MEH-PPV in PFO. These results indicate that MEH-PPV and PFO tend to be miscible with one another and do not undergo phase separation in the micron and submicron range.

TEM micrographs for the binary and ternary blends of MEH-PPV and PFO in PMMA with and without OsO_4 staining were carried out in order further elucidate the morphology. The samples were prepared by floating the films off PEDOT-PSS-coated glass substrates with deionized water onto a Cu grid. The lateral morphologies obtained by TEM for both the binary and ternary blends were similar to those observed by AFM and fluorescence microscopy as shown in Figure 3.

The contrast in the image obtained without OsO_4 is improved to a great extent when the MEH-PPV is

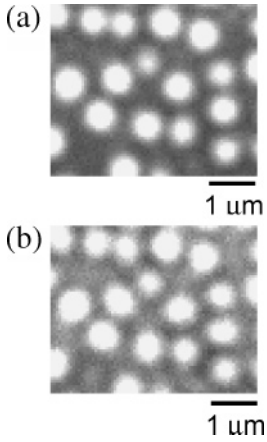

Figure 2. Photoluminescence images of 1:7 wt % of MEH-PPV:PFO in PMMA. (a) Excited with UV band-pass filter (360 nm ± 60 nm) and observed using a blue-violet transmitting (450 nm band-pass ± 40 nm) filter. (b) Excited with blue band-pass filter (425 ± 40 nm) and observed using a red transmitting (630 nm band-pass ± 60 nm) filter.

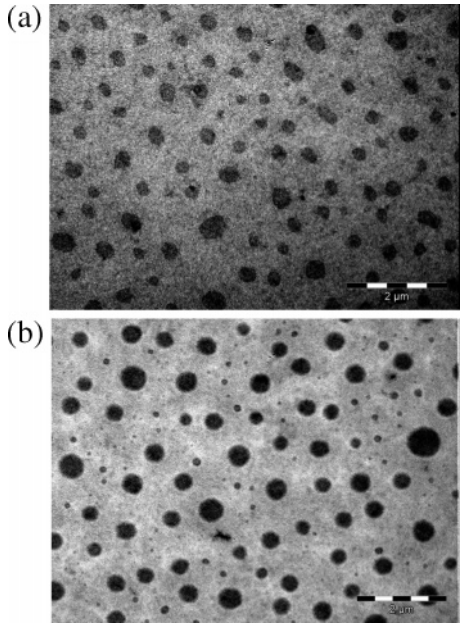

Figure 3. TEM images 1:7 wt % MEH:PFO in PMMA (a) without OsO_4 staining and (b) with OsO_4 staining.

stained with OsO_4 as shown by comparing parts b and a in Figure 3 for the 1:7 wt % blend of MEH-PPV:PFO in PMMA. OsO_4 specifically stains MEH-PPV due to the presence of the vinylene double bond and does not stain either PFO or PMMA. This further proves that the conjugated polymers are present together in the microdomains (400−600 nm) and are phase-separated from PMMA.

Photophysical Characteristics. Optical absorption and photoluminescence (PL) spectra of the films on PEDOT-PSS coated glass are shown in Figure 4a−d. Binary blends of PFO/PMMA have a λ_{max} at 390 nm and MEH-PPV/PMMA at 500 nm. The ternary blend systems show the absorption from both of the conjugated polymers as shown in Figure 4a as a function of blend composition. No new absorption features were observed, indicating that the blend components do not have any interactions in their electronic ground states. The magnitude of the absorption (0.01−0.04 AU) is low for these films as the total concentration of the conjugated

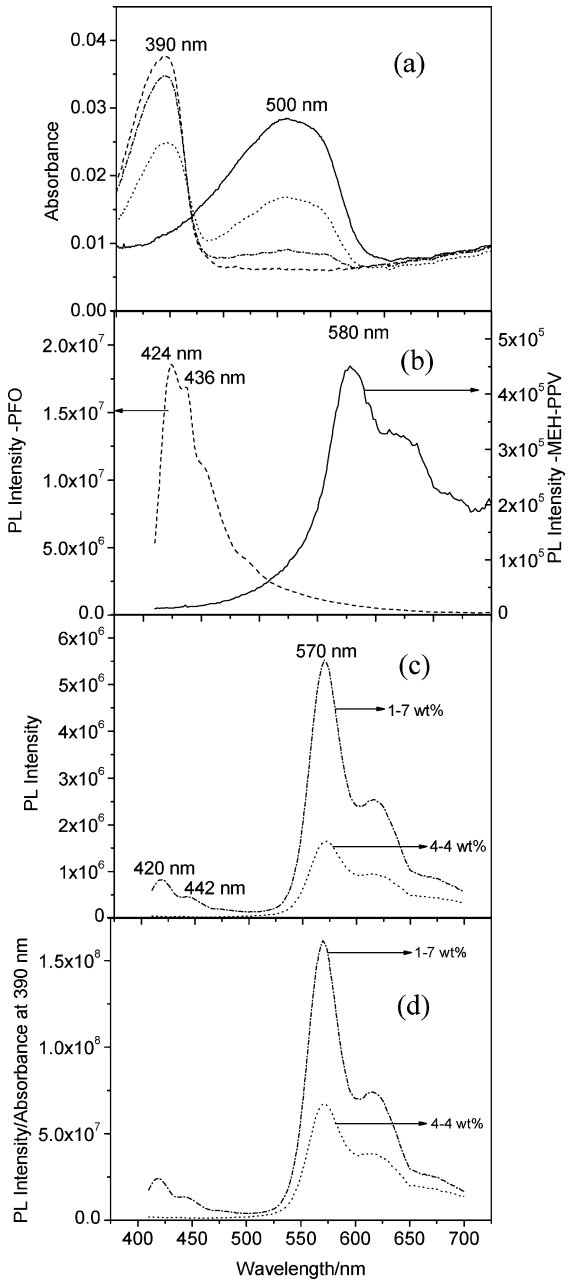

Figure 4. (a) Optical absorption spectra and (b) PL spectra of thin binary blend films of 8 wt % MEH-PPV and PFO in PMMA on PEDOT-PSS coated glass. (c) The PL emission of ternary blends of 4:4 wt % MEH-PPV:PFO and 1:7 wt % MEH-PPV:PFO in PMMA matrix. (d) Normalized emission intensity for the ternary blends. The excitation wavelength was 390 nm for the PL experiment. Legend: (—) 8 wt % MEH-PPV in PMMA; (- - -) 8 wt % PFO in PMMA; (• • •) 4:4 wt % MEH-PPV:PFO in PMMA; and (- • -) 1:7 wt % MEH-PPV:PFO in PMMA.

polymers (8 wt %) is low in the blends. PL spectra for the blends as shown in Figure 4b,c were taken by exciting the films at 390 nm where the absorption is mainly due to PFO and the MEH-PPV is poorly absorbing. The binary blend of PFO/PMMA show structured emission at 424 and 436 nm, while the MEH-PPV/PMMA blend shows a much weaker emission at 580 nm characteristic of MEH-PPV (Figure 4b). In the ternary blends (Figure 4c), the 4:4 wt % MEH-PPV:PFO in PMMA shows only a yellow-orange emission band at 570 nm mainly attributable to MEH-PPV emission with a blue shift possibly due to a decrease in aggregation of

Table 1. Device Characteristics for the Blend LEDs (ITO/PEDOT-PSS/Blends/Ca/Al)

composition (wt %)	V_{max} (V)	J (mA cm^{-2})	vis radiance (μW sr^{-1} cm^{-2})	luminance (cd/m^2)	ext QE ϕ_{ext}, %
8 wt % MEH-PPV in PMMA	8	226	37	221	0.05
4:4 wt % MEH-PPV:PFO in PMMA	12	806	24	160	0.01
1:7 wt % MEH-PPV:PFO in PMMA	11	914	24	162	0.01
8 wt % PFO in PMMA	11	879	30	4.6	0.008

the MEH-PPV when compared to the binary blend system. An increase in the intensity of MEH-PPV emission is observed in the ternary blend in comparison to the binary blends and can be attributed to Förster energy transfer from the excited state of PFO to MEH-PPV as the absorption spectrum of MEH-PPV overlaps with the PFO emission to a reasonable extent. Similar energy transfer has been reported for the binary blends of MEH-PPV and PFO without the matrix polymer.[33] Blends composed of 1:7 wt % of MEH-PPV:PFO in PMMA show more intense emission at 570 nm along with a weak emission at 420 and 442 nm corresponding to PFO. The increase in the intensity of the MEH-PPV emission relative to the 4:4 wt % ternary blend and 8 wt % MEH-PPV/PMMA binary blend indicates efficient Förster energy transfer, though it does not proceed to a complete extent as PFO emission is also observed. Figure 4d shows the normalized emission intensities with respect to the absorbance at 390 nm for the two ternary blends (4:4 and 1:7 wt % MEH-PPV:PFO in PMMA). On comparing parts c and d of Figure 4, it is seen that the emission intensity difference between the ternary blends is slightly reduced, and hence the increased photoluminescence of 1:7 wt % blend can be partly ascribed to its increased absorbance at the excitation wavelength 390 nm.

Electroluminescence from Binary and Ternary Blends. Light-emitting devices consisting of the binary and ternary blends of MEH-PPV, PFO, and PMMA sandwiched between an ITO/PEDOT-PSS anode and a Ca/Al cathode were constructed and examined between 0 and 12 V. The performance of these materials in EL devices was characterized by the current density−voltage ($J-V$) plots and the light output (radiance) as a function of operating voltage, as shown in Figure 5. In this instance, we choose to use radiance in μW cm^{-2} sr^{-1} as opposed to luminance in cd/m^2 as luminance values depend on the responsivity of the human eye, which is most sensitive to green color (ca. 555 nm) and changes with wavelength of emission. LEDs made from blends of MEH-PPV, PFO, and PMMA showed similar currents, though deviations were seen at higher voltages (~10−12 V) and elevated PFO content. The radiance values were found to be highest for the binary blend of MEH-PPV in PMMA, while the other blend compositions showed similar values. The overall radiance values are low relative to pure conjugated polymer-based devices, as expected from blends with only 8 wt % light-emitting polymer.

Table 1 summarizes the PLED performance results [maximum luminance (cd/m^2), radiance (μW sr^{-1} cm^{-2}) with corresponding operating voltage (V_{max}) and current density (J_{max}), along with external quantum efficiency (QE)] as a function of composition. The turn-on voltages for all devices was at 4 V, except for 8 wt % PFO in PMMA which turned on at 5 V as expected for a polymer with a higher band gap. The voltage at which the maximum brightness of the blend PLEDs were observed is shown in Table 1. It is seen that the ternary blend devices have improved brightness with values lying in between that of the MEH-PPV/PMMA and PFO/PMMA devices, where as the radiance values are slightly lesser than the binary blend devices. This can be attributed to the fact that radiance is independent of the color of the emission where as luminance being a photometric unit depends on the wavelength of emission and is maximum at 555 nm. PFO/PMMA devices show blue color where as the ternary blend devices show yellow/green color and hence have higher luminance values. Incorporation of MEH-PPV in PFO improves luminance and charge transport properties in the ternary blends. The external quantum efficiencies of the binary blends of MEH-PPV and PFO are 0.05% and 0.008%, respectively. The external quantum efficiencies of the ternary blends were similar and had a value of 0.01%. Though the phase-separated morphology is similar in both the binary and ternary blends, the amount of MEH-PPV in the blends directly affects their efficiency. Previously, nanophase-separated morphologies of MEH-PPV with poly(2,2′-(3,3′-dioctyl-2,2′-bithienylene)-6,6′-bis(4-phenylenequinoline)) (POBTPQ)[20] were reported to have external quantum efficiencies of 0.01% when the total concentration of MEH-PPV in the blends was 1−10 wt %. The values for external quantum efficiency observed in our work are comparable to these blends with the

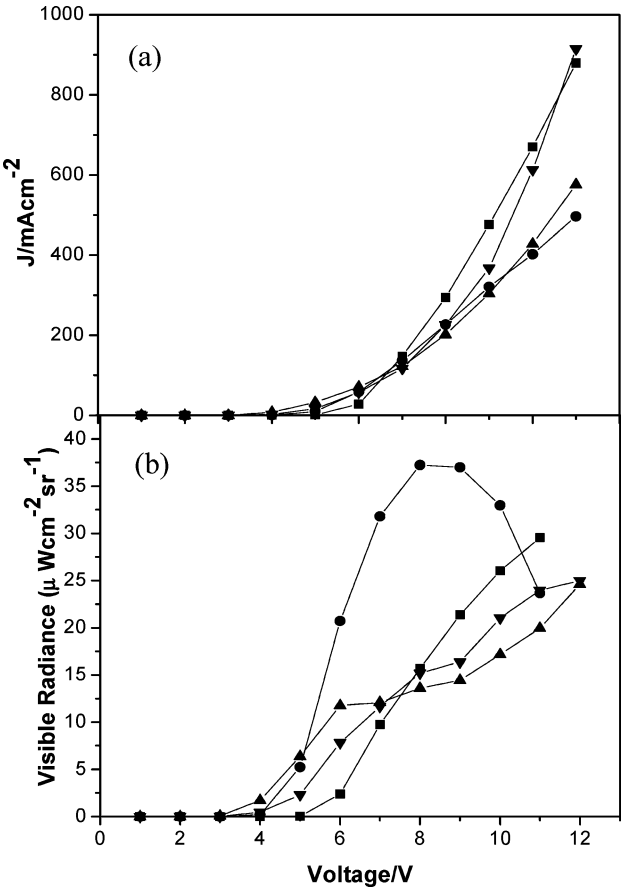

Figure 5. (a) Current density−voltage ($J-V$) and (b) radiance−voltage curves for binary and ternary blends of MEH-PPV and PFO in PMMA. Legend: (■) 8 wt % PFO in PMMA; (●) 8 wt % MEH-PPV in PMMA; (▲) 4:4 wt % MEH-PPV:PFO in PMMA; (▼) 1:7 wt % MEH-PPV:PFO in PMMA.

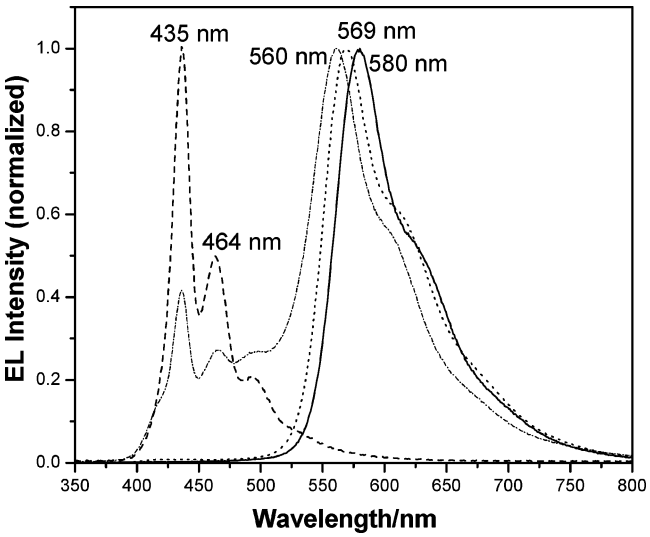

Figure 6. El spectra for the binary and ternary blends of MEH-PPV and PFO in PMMA at 10 V. Legend: (—) 8 wt % MEH-PPV in PMMA; (- - -) 8 wt % PFO in PMMA; (• • •) 4:4 wt % MEH-PPV:PFO in PMMA; and (- • -) 1:7 wt % MEH-PPV: PFO in PMMA.

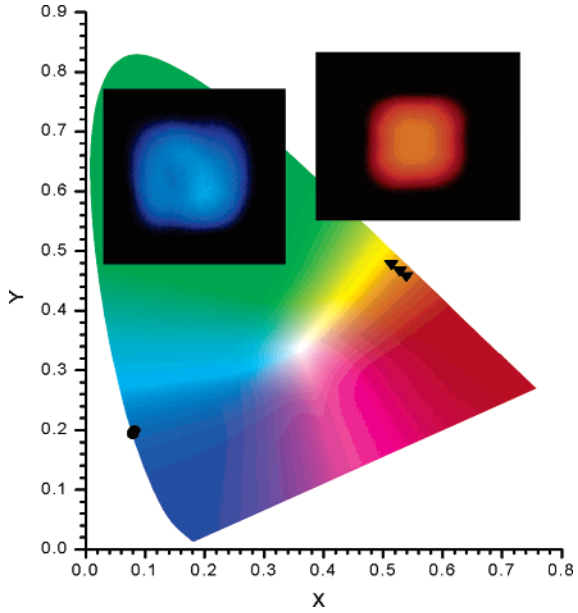

Figure 7. CIE 1931 diagram for 8 wt % PFO in PMMA (blue) and working device at 8 V along with 8 wt % MEH-PPV in PMMA (red-orange) and working device at 8 V.

difference being that the total concentration of conjugated polymers in our case is only 8 wt %. This indicates that, apart from the total concentration of the conjugated polymers, its distribution in the blend film plays an important role in charge injection and transport.

The EL emission spectra from the binary blends of MEH-PPV/PMMA and PFO/PMMA shown in Figure 6 are similar to the devices made from the homopolymers alone. Binary blends of MEH-PPV/PMMA showed the characteristic orange-red emission at 580 nm, and the corresponding CIE x, y coordinates are shown in Figure 7 along with a photograph of an emitting device. Binary blends of PFO/PMMA show the characteristic structured blue emission at 435, 464, and 492 nm (Figures 6 and 7). At elevated voltages of 11−12 V the peaks at 464 and 492 nm increased in intensity, and the long wavelength tail becomes more prevalent as the light begins whitening. These emission broadening effects

Scheme 2

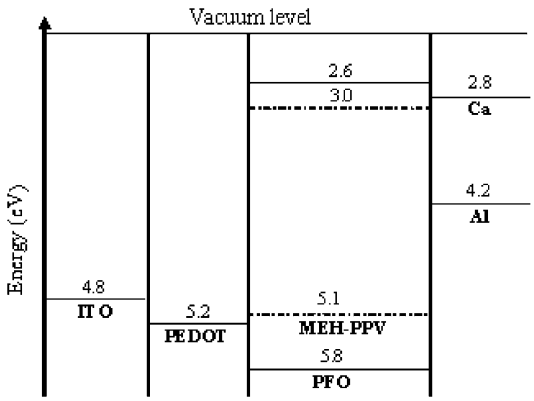

and spectral instability of PFO are well-studied and have been reported by numerous groups.[40] In general, blending of PFO with an insulating polymer (e.g., PMMA) suppresses this effect to a certain extent as the device remains blue-emitting to higher voltages as evidenced when PFO was blended with PS and poly(vinyldiphenylquinoline) (PVQ).[41] The corresponding CIE coordinates shown in Figure 7 with an image of a working device at 8 V clearly show this blue color.

Scheme 2 shows a schematic of the HOMO and LUMO energy levels of MEH-PPV and PFO relative to ITO at 4.8 eV and PEDOT-PSS at 5.2 eV.[42] The band gaps for PFO[25] and MEH-PPV are 3.2 and 2.1 eV, respectively, as calculated from the HOMO−LUMO energy difference, showing that the HOMO and LUMO energy levels of MEH-PPV are nested in between the energy levels of PFO, suggesting favorable energy transfer from PFO to MEH-PPV in accordance with Scheme 1.

The ternary blends containing an equal concentration of MEH-PPV and PFO (4:4 wt %) in PMMA have an emission at 569 nm as shown in Figure 6 and was found to be invariant with applied voltage. The EL spectrum is identical to its PL spectrum and confirms Förster energy transfer from the PFO to the MEH-PPV. These EL devices showed a predominantly yellow emission; the corresponding CIE coordinates are shown in Figure 8a, and photographs of the working devices at different voltages are shown in Figure 8b. The saturation value for the devices changes as the voltage is increased as evidenced by a shift of CIE coordinates. The ternary blend having an excess concentration of PFO relative to MEH-PPV (1:7 wt %) showed a distinct voltage-based color tunable LED. The EL spectra in Figure 6 show emission at 435, 464, and 560 nm at 10 V. At lower voltages (6−9 V), the device exhibits a yellow emission with λ_{max} at 560 nm corresponding to MEH-PPV dominant emission which is blue-shifted when compared to its PL spectrum. It has been seen that, as MEH-PPV concentration decreases, its emission spectrum consistently shifts to the blue.[33] As the voltage is further increased, emission rises in the blue region of the spectrum corresponding to the PFO component. This changes the color of the emission from yellow to green, as seen in the device photograph in Figure 8c. The change in color with voltage is also seen in the CIE coordinates in Figure 8a which traces the points from a yellow under low voltages to a green at higher voltage. In considering the origin of these color changes, we attribute the yellow emission to Förster energy transfer from PFO to MEH-PPV. As the voltage is increased,

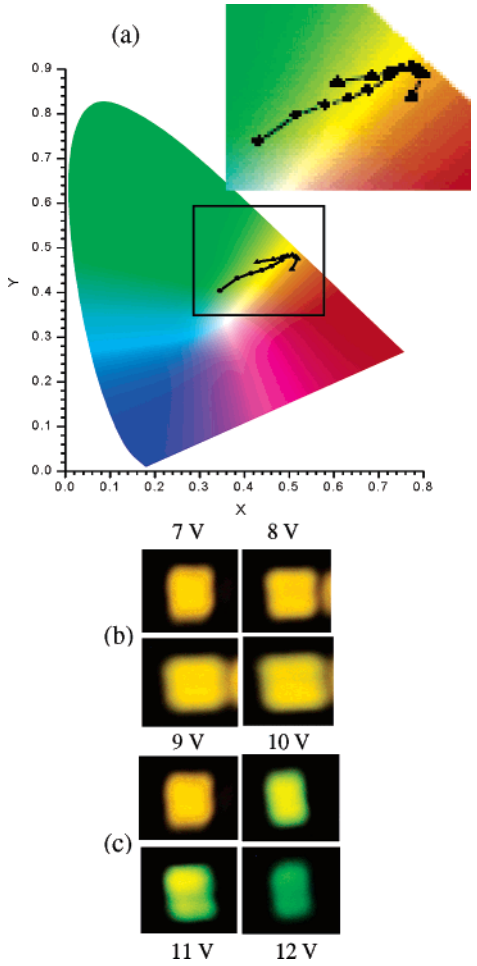

Figure 8. (a) CIE 1931 diagram for 4:4 wt % MEH-PPV:PFO in PMMA and 1:7 wt % MEH-PPV:PFO in PMMA. Inset: expanded portion of the CIE diagram indicating the change in color with voltage. Legend: (●) 4:4 wt % MEH-PPV:PFO in PMMA; (▲) 1:7 wt % MEH:PPV:PFO in PMMA. (b) Electroluminescence from 4:4 wt % MEH-PPV:PFO in PMMA at different voltages. (c) Electroluminescence from 1:7 wt % MEH-PPV:PFO in PMMA at different voltages.

exciton formation and recombination also occurs on the PFO in the microdomains which gives its characteristic blue emission, thus summing to green. It is seen that even at very low concentrations of MEH-PPV in the ternary blends, energy transfer is predominant and the device gives mainly on MEH-PPV emission. The PFO emission is low when compared to the emission from the MEH-PPV domain as seen in Figure 6 but is still high enough to influence the color of the devices.

Inversion of morphology occurred as the compositions of conjugated polymers were increased with respect to PMMA. When considering higher compositions (ca. 50 wt %) of total conjugated polymer in PMMA, the conjugated polymers form the matrix, and PMMA blooms up as micro- and nanodomains on the conjugated polymer surface as shown by the AFM topographic images in Figure 9. At these compositions, the ternary blend devices show a predominantly yellow color and no separate blue emission from PFO is observed. With increased voltage, no change to green emission or color tuning is evident. This indicates that a morphology in which domains of the conjugated polymers exists in the insulating matrix is essential to achieving voltage tunable multicolor emission. In our studies, it was also seen that the relative concentration of the conjugated polymers in the domains plays an important role in determining the emission color as well as its tunability. In the case of a PLED consisting of 4:4 wt % MEH-PPV:PFO in PMMA, a predominantly yellow color emission was observed, while color tuning occurred in the ternary blend having 1:7 wt % of MEH-PPV:PFO in PMMA even though both compositions showed a similar morphology. In a previous study, phase separation between the conjugated polymers was found to be essential in achieving voltage tunable multiccolor emission.[20] In our study, color tuning is seen to occur even though the conjugated polymers are present together in a single domain. It is very difficult to identify if the conjugated polymers in the 1:7 wt % MEH-PPV:PFO in PMMA device are phase-separated within the microdomain. Neither TEM nor fluorescence microscopy shows any evidence of phase separation between MEH-PPV and PFO in a single domain measured to a resolution of 100 nm. In the ternary blends, the conjugated polymers seem to be compatible in the microdomain, and the emission is dependent on the compositional ratio between them as discussed in Scheme 1. It is seen that morphology, as well as the interaction between the conjugated polymers, plays an important role in color tuning.

Conclusions

Binary and ternary blends of MEH-PPV and PFO in PMMA were found to exhibit nano- and microdomains of 100−600 nm in diameter depressed into the surface. It was observed that interplay between the solubility parameters of the polymer components and the solvent is important for controlling the morphology of these phase-separated blends. Quenching of PFO emission due to Förster energy transfer from PFO to MEH-PPV was found to be present in the ternary blends having greater than or equal to composition of PFO relative to

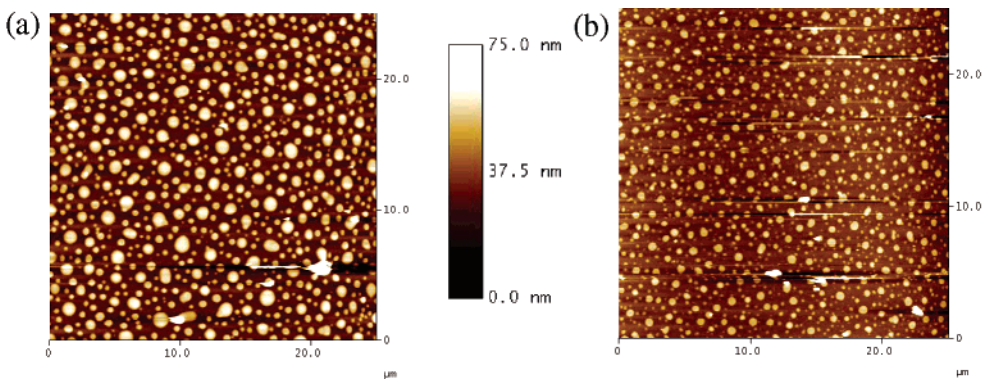

Figure 9. AFM topographic images of (a) 25:25 and (b) 37.5:37.5 wt % of MEH-PPV:PFO in PMMA.

MEH-PPV in PMMA. A phase-separated morphology, as well as the composition of the conjugated polymers, controls the ability to obtain a voltage-controlled variable color PLED. Further studies are being carried out in order to improve the efficiency of these phase-separated LEDs. The technical possibilities for these PLEDs are enormous as light sources of variable color and intensity can be produced. Phase separation in polymer blends provides easy accessibility to voltage-controlled multicolor color emission for PLEDs leading to new directions in polymer electronics and opens up a multitude of venues for preparing PLEDs at low cost.

Experimental Section

Materials and Preparation of Blend Films. PMMA (M_w = 82 kDa) was purchased from Aldrich and was used as received. MEH-PPV (M_w = 140 kDa) was synthesized as previously reported,[32] and PFO (M_w = 100 kDa) was purchased from American Dye Source. The individual polymer solutions were prepared by dissolving the homopolymers in toluene at a concentration of 5 mg/mL. Polymer blend solutions were prepared by mixing the corresponding homopolymer solutions to obtain the required composition. Glass substrates (Corning cover-glass, 25 mm^2) were cleaned in an ultrasonic bath with aqueous sodium dodecyl sulfate (SDS) (Fisher, Versa-Clean solution), acetone, and methanol and were used for AFM and fluorescence and TEM measurements. They were first spin-coated with PEDOT-PSS (Bayer Baytron P VP Al 4083) at 4000 rpm and dried under vacuum for 2 h at 150 °C. The polymer blend films were prepared by spin-coating at 1000 rpm for 30 s. Thickness measurements were made with a Dektak 3030 profilometer over several points on each sample to yield an average thickness of 80−100 nm for all films. TEM samples were prepared by floating the films off of the glass-coated PEDOT-PSS substrates with deionized water from to a Cu grid.

Morphology Characterization. Tapping-mode AFM was carried out using a Nanoscope IIIa Dimension 3100. Fluorescence microscopy images were taken using an Olympus IX70 fitted with a 100 W Hg source (USH-102DH) and a CCD camera (Princeton, RTE 1300 × 1030) mounted on the side port. Fluorescence microscopy was carried out with a blue-violet modular filter cube (Chroma Technology, excitation 425 nm, 40 nm band-pass; emission 630 nm, 60 nm band-pass; 475 nm dichroic splitter) and UV modular filter cube (Chroma Technology, excitation 360 nm, 40 nm band-pass; emission 420 nm, 40 nm band-pass; 400 nm dichroic splitter). Fluorescence images were collected through 10× and 40× objective lenses (Olympus U Plan Fl, 0.30NA and SLC Plan Fl, 0.55NA, respectively). A blue-violet (425 nm band-pass ± 40 nm) and UV filter (360 nm ± 40 nm) was used to filter the excitation source, and a red (630 nm band-pass ± 60 nm) and blue filter (450 nm band-pass ± 40 nm) was used to filter the emission light for obtaining the fluorescence images. TEM measurements were done using a Hitachi H-7000 TEM at acceleration voltage of 75 kV under bright-field mode.

Photophysics and Electroluminescence Measurements. Optical absorption spectra were obtained using a Cary UV−vis−near-IR spectrophotometer. Photoluminescence measurements on blend films were carried out on a FluoroLog-3 spectrofluorometer. The thin films were faced positioned front face (90°) from the incident beam. Electroluminescent devices were prepared by etching masked ITO glass (Delta Technologies, R_s = 8−12 Ω/□) by exposure to aqua regia vapor. The etched substrate was cleaned in an ultrasonic bath with aqueous sodium dodecyl sulfate (SDS) (Fisher, Versa-Clean solution), Milli-Q water, acetone, and 2-propanol. This was followed by spin-coating with PEDOT/PSS and drying as described above. The polymer blend solutions were then spin-coated, and the resulting films were dried under vacuum (1×10^{-6} Torr) for 12 h at room temperature. Calcium (50 Å) and aluminum (2000 Å) were sequentially deposited by thermal evaporation on the polymer film. After deposition, the devices were encapsulated with epoxy. All device measurements were carried out at room temperature. The active area on the etched ITO was 0.07 cm^2. Spectral measurements were carried out on an ISA-SPEX Triax 180 spectrograph fitted with a liquid N_2 cooled CCD detector (EEV back-illuminated CCD, 1024 × 128 pixels, 400−1100 nm). A secondary standard tungsten lamp was used to calibrate the CCD detector. Measurements were made normal to the surface of the devices, and in the computation of EL quantum efficiencies it was assumed that the spatial distribution was Lambertian.[43] External device quantum efficiencies were calculated as described in the literature.[44]

Acknowledgment. This work was supported by Army Research Laboratory Grant W911NF-04-200023 through the Advanced Carbon Nanotechnology Program.

References and Notes

(1) Burroughes, J. H.; Bradley, D. D. C.; Brown, A. R.; Marks, R. N.; Mackay, K.; Friend, R. H.; Burns, P. L.; Holmes, A. B. *Nature (London)* **1990**, *347*, 539.
(2) Braun, D.; Heeger, A. J. *Appl. Phys. Lett.* **1991**, *58*, 1982.
(3) Kraft, A.; Grimsdale, A. C.; Holmes, A. B. *Angew. Chem., Int. Ed.* **1998**, *37*, 402.
(4) Friend, R. H.; Gymer, R. W.; Holmes, A. B.; Burroughes, J. H.; Marks, R. N.; Taliani, C.; Bradley, D. D. C.; Dos Santos, D. A.; Bredas, J. L.; Logdlund, M.; Salaneck, W. R. *Nature (London)* **1999**, *397*, 121.
(5) Wang, Y. Z.; Sun, R. G.; Wang, D. K.; Swager, T. M.; Epstein, A. J. *Appl. Phys. Lett.* **1999**, *74*, 2593.
(6) Huang, C. C.; Meng, H. F.; Ho, G. K.; Chen, C. H.; Hsu, C. S.; Huang, J. H.; Horng, S. F.; Chen, B. X.; Chen, L. C. *Appl. Phys. Lett.* **2004**, *84*, 1195.
(7) Jin, S.-H.; Kang, S.-Y.; Yeom, I.-S.; Kim, J. Y.; Park, S. H.; Lee, K.; Gal, Y.-S.; Cho, H.-N. *Chem. Mater.* **2002**, *14*, 5090.
(8) Gowri, R.; Mandal, D.; Shivkumar, B.; Ramakrishnan, S. *Macromolecules* **1998**, *31*, 1819.
(9) Ego, C.; Marsitzky, D.; Becker, S.; Zhang, J.; Grimsdale, A. C.; Muellen, K.; MacKenzie, J. D.; Silva, C.; Friend, R. H. *J. Am. Chem. Soc.* **2003**, *125*, 437.
(10) Moons, E. *J. Phys.: Condens. Matter* **2002**, *14*, 12235.
(11) Gong, X.; Ma, W.; Ostrowski, J. C.; Bazan, G. C.; Moses, D.; Heeger, A. J. *Adv. Mater.* **2004**, *16*, 615.
(12) Hwang, D.-H.; Park, M.-J.; Kim, S.-K.; Lee, N.-H.; Lee, C.; Kim, Y.-B.; Shim, H.-K. *J. Mater. Res.* **2004**, *19*, 2081.
(13) Ding, L.; Karasz, F. E.; Lin, Z.; Zheng, M.; Liao, L.; Pang, Y. *Macromolecules* **2001**, *34*, 9183.
(14) Kim, J.-S.; Ho, P. K. H.; Murphy, C. E.; Friend, R. H. *Macromolecules* **2004**, *37*, 2861.
(15) Morgado, J.; Moons, E.; Friend, R. H.; Cacialli, F. *Synth. Met.* **2001**, *124*, 63.
(16) Nishino, H.; Yu, G.; Heeger, A. J.; Chen, T. A.; Rieke, R. D. *Synth. Met.* **1995**, *68*, 243.
(17) Shim, H. K.; Kang, I. N.; Jang, M. S.; Zyung, T.; Jung, S. D. *Macromolecules* **1997**, *30*, 7749.
(18) Ding, L.; Karasz, F. E.; Lin, Y.; Pang, Y.; Liao, L. *Macromolecules* **2003**, *36*, 7301.
(19) Zhang, X.; Jenekhe, S. A. *Macromolecules* **2000**, *33*, 2069.
(20) Alam, M. M.; Tonzola, C. J.; Jenekhe, S. A. *Macromolecules* **2003**, *36*, 6577.
(21) Berggren, M.; Inganas, O.; Gustafsson, G.; Rasmusson, J.; Andersson, M. R.; Hjertberg, T.; Wennerstrom, O. *Nature (London)* **1994**, *372*, 444.
(22) Anni, M.; Gigli, G.; Paladini, V.; Cingolani, R.; Barbarella, G.; Favaretto, L.; Sotgiu, G.; Zambianchi, M. *Appl. Phys. Lett.* **2000**, *77*, 2458.
(23) Tasch, S.; List, E. J. W.; Ekstrom, O.; Graupner, W.; Leising, G.; Schlichting, P.; Rohr, U.; Geerts, Y.; Scherf, U.; Mullen, K. *Appl. Phys. Lett.* **1997**, *71*, 2883.
(24) List, E. J. W.; Tasch, S.; Hochfilzer, C.; Leising, G.; Schlichting, P.; Rohr, U.; Geerts, Y.; Scherf, U.; Mullen, K. *Opt. Mater.* **1998**, *9*, 183.
(25) Charas, A.; Morgado, J.; Martinho, J. M. G.; Fedorov, A.; Alcacer, L.; Cacialli, F. *J. Mater. Chem.* **2002**, *12*, 3523.
(26) Parker, I. D. *J. Appl. Phys.* **1994**, *75*, 1656.
(27) He, G.; Li, Y.; Liu, J.; Yang, Y. *Appl. Phys. Lett.* **2002**, *80*, 4247.

(28) Granström, M.; Inganäs, O. *Adv. Mater.* **1995**, *7*, 1012.
(29) Granström, M.; Berggren, M.; Inganäs, O. *Science* **1995**, *267*, 1479.
(30) Iyengar, N. A.; Harrison, B.; Duran, R. S.; Schanze, K. S.; Reynolds, J. R. *Macromolecules* **2003**, *36*, 8978.
(31) Granström, M.; Berggren, M.; Inganäs, O.; Andersson, M. R.; Hjertberg, T.; Wennerstörm, O. *Synth. Met.* **1997**, *85*, 1193.
(32) Padmanaban, G.; Ramakrishnan, S. *J. Am. Chem. Soc.* **2000**, *122*, 2244.
(33) Liu, J.; Shi, Y.; Yang, Y. *Appl. Phys. Lett.* **2001**, *79*, 578.
(34) Sprenger, M.; Walheim, S.; Budkowski, A.; Steiner, U. *Interfacial Sci.* **2003**, *11*, 225.
(35) Wang, P.; Koberstein, J. T. *Macromolecules* **2004**, *37*, 5671.
(36) Van Krevelen, D. W. *Properties of Polymers: Their Correlation with Chemical Structure; Their Numerical Estimation and Prediction from Additive Group Contributions*; Elsevier: Amsterdam, 1990.
(37) Walheim, S.; Boeltau, M.; Mlynek, J.; Krausch, G.; Steiner, U. *Macromolecules* **1997**, *30*, 4995.
(38) Affrossman, S.; Henn, G.; O'Neill, S. A.; Pethrick, R. A.; Stamm, M. *Macromolecules* **1996**, *29*, 5010.
(39) Chappell, J.; Lidzey, D. G. *J. Microsc.* **2003**, *209*, 188.
(40) Sims, M.; Ariu, M.; Asimakis, A.; Koeberg, M.; Stouff, M.; Fox, M.; Bradley, D. D. C. *Proc. SPIE—Int. Soc. Opt. Eng.* **2004**, *5214*, 216. (b) Kulkarni, A. P.; Kong, X.; Jenekhe, S. A. *J. Phys. Chem. B* **2004**, *108*, 8689. (c) Gong, X.; Moses, D.; Heeger, A. J.; Xiao, S. *Synth. Met.* **2004**, *141*, 17. (d) Gamerith, S.; Gadermaier, C.; Scherf, U.; List, E. J. W. *Phys. Status Solidi A* **2004**, *201*, 1132.
(41) Kulkarni, A. P.; Jenekhe, S. A. *Macromolecules* **2003**, *36*, 5285.
(42) Brown, T. M.; Kim, J. S.; Friend, R. H.; Cacialli, F.; Daik, R.; Feast, W. J. *Appl. Phys. Lett.* **1999**, *75*, 1679.
(43) Greenham, N. C.; Friend, R. H.; Bradley, D. D. C. *Adv. Mater.* **1994**, *6*, 491.
(44) He, Y.; Hattori, R.; Kanicki, J. *Rev. Sci. Instrum.* **2000**, *71*, 2104.

MA050787J